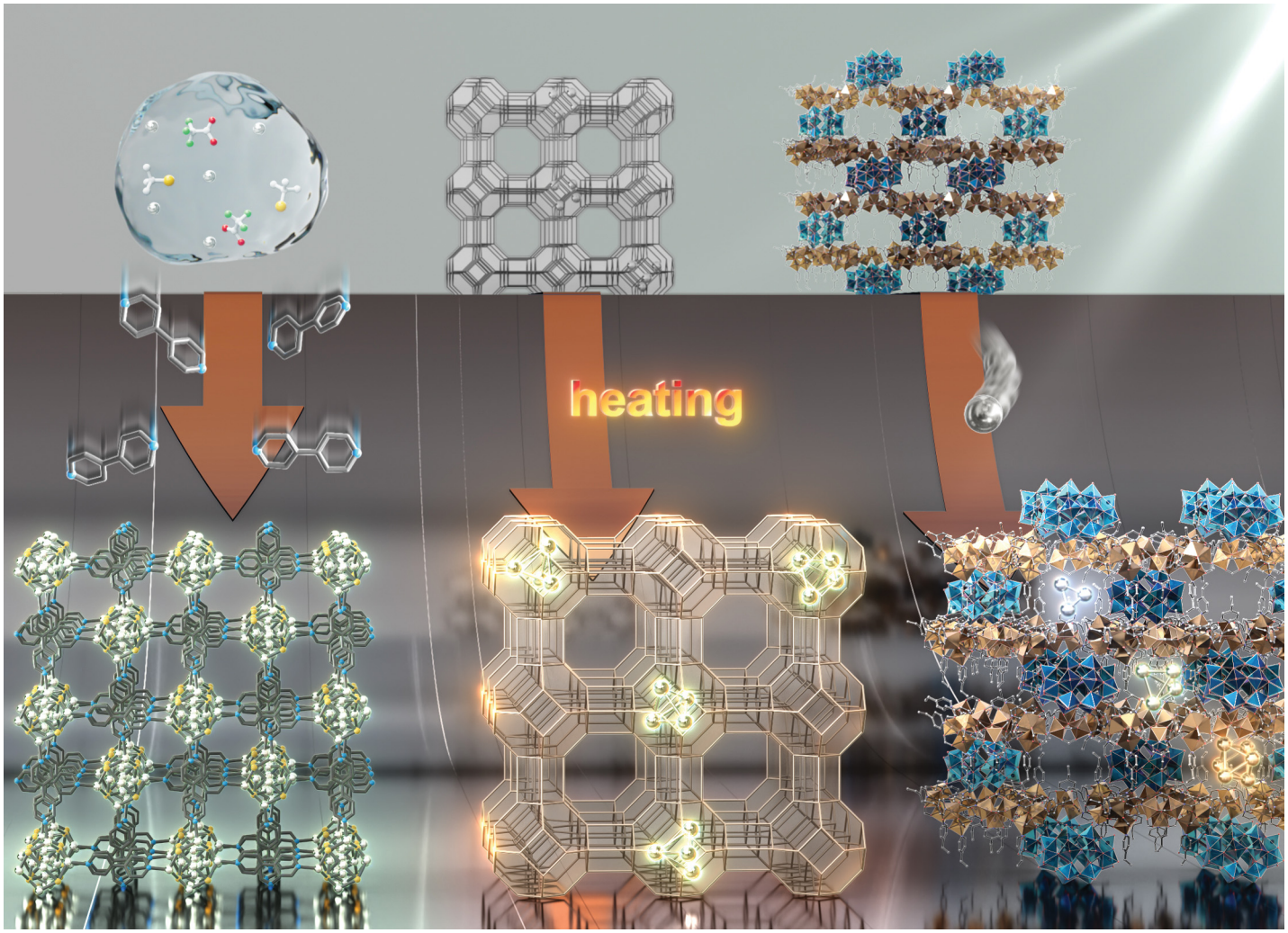

Showcasing research from Professor Sayaka Uchida's laboratory, School of Arts and Sciences, The University of Tokyo, Japan

Small luminescent silver clusters stabilized in porous crystalline solids

Subnanometric or small metal clusters (SMCs) have been extensively researched due to their unique electronic, optical, catalytic, and magnetic properties, which are different from the bulk samples. In this review, we provide an overview of the synthesis, structures, and luminescent properties of Ag clusters in porous crystalline solids such as metal–organic frameworks (MOFs), zeolites, and porous ionic crystals (PICs).

As featured in:

See Sayaka Uchida *et al.*, *Phys. Chem. Chem. Phys.*, 2024, **26**, 6512.

ROYAL SOCIETY OF CHEMISTRY

rsc.li/pccp

Registered charity number: 207890

PCCP Owner Societies

PCCP

ROYAL SOCIETY OF CHEMISTRY

PERSPECTIVE

View Article Online
View Journal | View Issue

Cite this: *Phys. Chem. Chem. Phys.*, 2024, **26**, 6512

Small luminescent silver clusters stabilized in porous crystalline solids

Naoya Haraguchi, Taisei Kurosaki and Sayaka Uchida *

Received 21st September 2023,
Accepted 8th January 2024

DOI: 10.1039/d3cp04589g

rsc.li/pccp

Subnanometric or small metal clusters (SMCs) have been extensively researched due to their unique electronic, optical, catalytic, and magnetic properties, which differ from those of bulk samples. Among the SMCs, silver (Ag) clusters have received significant interest due to their affordability and unique luminescent properties. Currently, two major approaches, gas-phase and liquid-phase synthesis, have been employed to obtain Ag clusters with precise control of size and structure. More recently, attention has been directed toward the utilization of porous crystalline solids such as metal–organic frameworks (MOFs), zeolites, and porous ionic crystals (PICs) to synthesize and stabilize Ag clusters. In this review, we aim to provide a comprehensive overview of the synthesis, structures, and luminescent properties of Ag clusters in porous crystalline solids.

1. Introduction

Subnanometric metal clusters, commonly referred to as small metal clusters (SMCs), have been intensively studied due to their unique electronic, optical, catalytic, or magnetic properties, stemming from their discrete electronic structure, distinctive atomic arrangements, and high surface-to-atom ratio, which are not observed in the corresponding bulk samples.[1,2] Since the properties of SMCs are highly dependent on size (nuclearity or number of atoms), structure, and types of protecting ligands, it is important to control these parameters to fine-tune their properties. SMCs exhibit a molecule-like behavior due to their discrete electronic energy levels. Consequently, well-defined transitions with energies in the visible light region can occur, enabling strong fluorescence in some of these clusters. A landmark example was reported by Zheng, Dickson, and co-workers showing that water-soluble few-atom Au clusters encapsulated in poly(amidoamine) dendrimers exhibit size-dependent specific fluorescence (Au_5 (UV), Au_8 (blue), Au_{13} (green), Au_{23} (red)).[3] Among the numerous reports on luminescent SMCs, considerable attention has been directed toward Ag clusters due to their relatively low price and distinctive color tone and luminescence properties different from their gold counterparts.[4,5]

Meanwhile, gas-phase synthesis is one of the most commonly employed methods for synthesizing small Ag clusters.[6] Within this approach, monodispersed small Ag clusters can be obtained through size-separation of clusters of various sizes generated by sputtering or vaporization. However, the yield of clusters is markedly low, and this method necessitates sophisticated equipment. Therefore, gas-phase synthesis is impractical for real-world applications of small Ag clusters. Another method involves the use of protecting ligands in the liquid phase.[7] Ag ions are reduced by reducing reagents, and Ag clusters subsequently form, which are stabilized by the protecting ligands.

On the other hand, synthetic approaches have emerged to form and stabilize small Ag clusters in porous crystalline solids such as metal–organic frameworks (MOFs)[8] and zeolites.[4] The formation of small Ag clusters in the solid-phase offer the advantage of improved stability, resulting in a higher density or weight percentage of Ag clusters and an increase in luminescence intensity and efficiency. In addition, it is expected that the luminescence properties can be controlled by the solvent molecules adsorbed in the pores of crystalline solids (*i.e.*, solvatochromism or vapochromism).[9]

Despite the large numbers of papers on small luminescent Ag clusters formed and stabilized in porous crystalline solids, to the best of our knowledge, there is no comprehensive review on this subject. The photophysical properties of Ag clusters, including the origin of photoluminescence (PL) in Ag clusters, particularly those formed in zeolites, have already been reported in papers and reviews.[10,11] However, the synthetic methods employed for Ag clusters, which significantly influence their physical properties, have not yet been systematically categorized to date. We have recently reported the synthesis of luminescent small Ag clusters *via* electron transfer in redox-active porous ionic crystals.[12–14] Therefore, the purpose of this perspective is to systematically categorize these composites and to provide an overview of the synthesis, structures, and

Department of Basic Science, School of Arts and Sciences, The University of Tokyo 3-8-1 Komaba, Meguro-ku, Tokyo 153-8902, Japan. E-mail: csayaka@g.ecc.u-tokyo.ac.jp

luminescent properties of small Ag clusters formed and stabilized in porous crystalline solids.

2. Silver cluster-containing MOFs

2.1. Ag clusters as framework nodes of MOFs

MOFs are porous crystalline materials constructed by the assembly of metal ions/clusters and organic linkers through coordination bonds. Ag chalcogenide/chalcogenolate cluster-based MOF (SCC-MOF) was first reported by Huang, Zang, and co-workers in 2017[8] by using a luminescent SCC $[Ag_{12}(S^tBu)_6(CF_3COO)_6(CH_3CN)_6]\cdot CH_3CN$ (**Ag_{12}**). A SCC-MOF $[(Ag_{12}(S^tBu)_8(CF_3COO)_4(bpy)_4)]_n$ (**Ag_{12}bpy**) was obtained by replacing the CH_3CN ligand in **Ag_{12}** with a bidentate 4,4′-bipyridine (bpy) linker. The Ag clusters in **Ag_{12}bpy** were linked to each other by bpy. While **Ag_{12}** exhibited a three-layered structure of Ag_5S_2–Ag_2S_2–Ag_5S_2 (Fig. 1a), the middle layer changed from a square pyramidal Ag_2S_2 configuration to a tetrahedral Ag_2S_4 configuration by the formation of **Ag_{12}bpy** (Fig. 1b). The stability of the Ag cluster remarkably increased by the ligand replacement, and the PL quantum yield (PLQY) improved from 0.2% to 12.1%. In the case of **Ag_{12}bpy**, the luminescence originated from the triplet state, which rapidly turned off by O_2. Additionally, **Ag_{12}bpy** showed a bright green emission under vacuum, and multi-color switching of luminescence was realized by solvatochromism/vapochromism with volatile organic compounds (VOCs). The emission color under the VOCs red-shifted with the increase in their polarity. These results show that incorporating SCC into the MOF framework led to enhanced stability and acquisition of multi-color luminescent characteristics.

After this study, Dong, Zang, and co-workers demonstrated that the luminescent properties of SCC-MOFs can be tuned by functional modification of the MOF linker. They reported the synthesis of $[(Ag_{12}(S^tBu)_8(CF_3COO)_4(bpy\text{-}NH_2)_4)]_n$ (**Ag12bpy-NH_2**, Fig. 1b), which is isostructural with **Ag12bpy**,[15] where the Ag_{12} cluster units were analogous by modifying the bpy linker with 3-amino-4,4′-bipyridine (**bpy-NH_2**). It has been known that pristine **bpy-NH_2** in the solid state emits blue fluorescence.[16] **Ag_{12}bpy-NH_2** exhibited dual emission of yellow phosphorescence (Ph) and blue fluorescence (Fl), while **Ag_{12}bpy** emitted green Fl. As in the case of **Ag_{12}bpy**, the Ph of **Ag_{12}bpy-NH_2** is quenchable with O_2, but the detection limit is much lower (32 Pa for **Ag_{12}bpy** and 11.4 mPa for **Ag_{12}bpy-NH_2**). Additionally, the authors synthesized **Ag_{12}bpy-CH_3**, which is isostructural with **Ag_{12}bpy** and **Ag_{12}bpy-NH_2**, but insensitive to oxygen. Therefore, **bpy-NH_2** and **bpy-CH_3** linkers contribute to increasing and decreasing, respectively, the sensitivity of Ph toward O_2. Moreover, the O_2-sensing pressure can be controlled by mixing and changing the ratio of **bpy-NH_2** and **bpy-CH_3** linkers in the MOF.

The luminescent properties of SCC-MOFs can be tuned by altering the geometric/electronic structure of the Ag cluster. For instance, Huang, Zang, and co-workers reported that isomerization of the Ag cluster occurs when dissolving **Ag_{12}bpy** in *N*,*N*-dimethylacetamide (DMAc)/toluene (3 : 1), resulting in the formation of **Ag_{12}bpy-2** (Fig. 1c).[16] This transformation changes

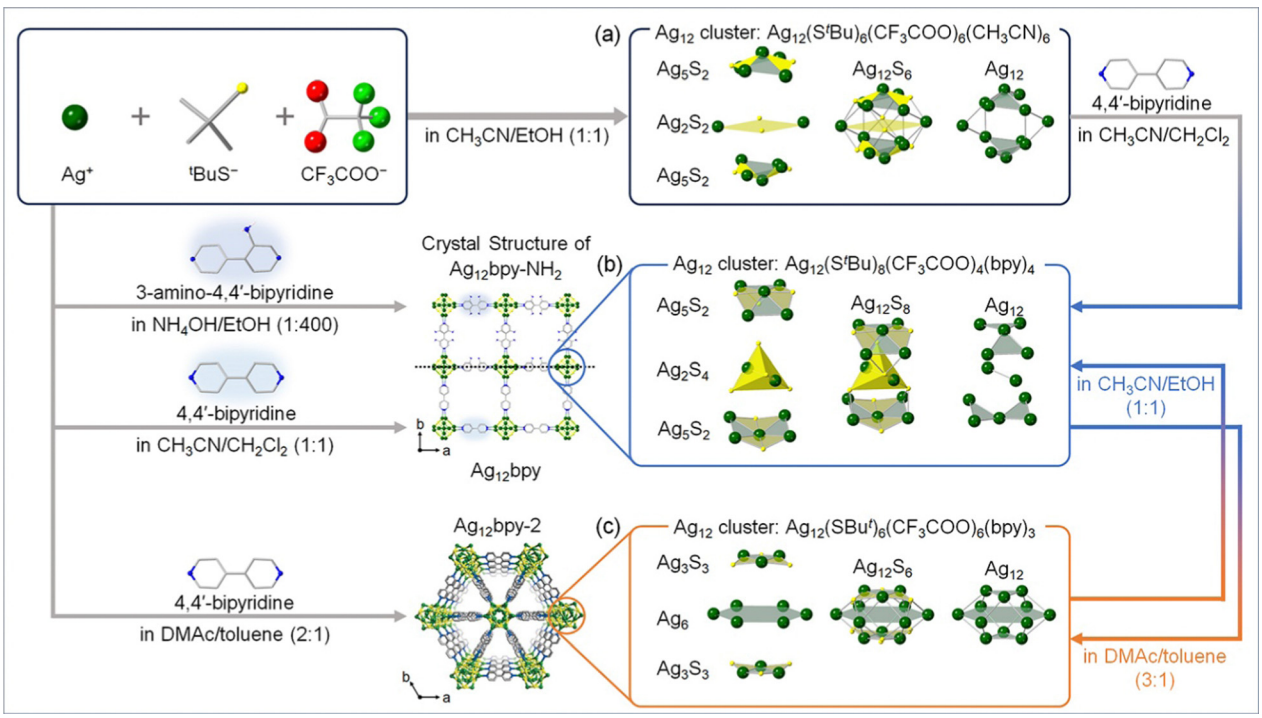

Fig. 1 Design approach and schematic illustration of the syntheses and structures of **Ag_{12}**-based SCC-MOFs. (a) **Ag_{12}**, (b) **Ag_{12}bpy** and **Ag_{12}bpy-NH_2**, and (c) **Ag_{12}bpy-2**.

the Ag cluster from a three-layered structure to a compressed empty cuboctahedron. Notably, **Ag_{12}bpy** and **Ag_{12}bpy-2** exhibited distinct luminescence, with a single green emission for **Ag_{12}bpy** and a dual blue-red emission for **Ag_{12}bpy-2**. Subsequently, the authors conducted DFT calculations to gain insight into the structure–luminescence relationship. The results indicated that for **Ag_{12}bpy**, degenerated LUMO–LUMO+7, characterized by π* orbitals of the bpy ligands, appeared. In contrast, for **Ag_{12}bpy-2** with a compressed cuboctahedron, Ag cluster-centered LUMO as well as LUMO+1–+6 with close energies distributed on the bpy ligands appeared. Combining these findings with time-dependent DFT calculations, the dual phosphorescence of **Ag_{12}bpy-2** with respective maxima at 463 nm and 620 nm can be deduced to originate from two separate excited states arising mainly from Ag cluster-centered transitions and intraligand transitions, respectively.

2.2. Ag clusters formed inside the pores of MOFs

Houk, Allendorf, and co-workers reported the formation of Ag clusters inside the pores of three water-stable MOFs, Cu(BTC), MOF-508, and MIL-68(In), by infiltrating them in an aqueous-ethanolic solution of $AgNO_3$, where ethanol could reduce Ag^+ to Ag^0 *in situ*.[17] EPR spectroscopy indicated that the Ag clusters formed in MOF-508 and MIL68(In) were linear $[Ag_3]^0$, which were particularly abundant in MOF-508. As shown in Fig. 2, Tiburcio, Pardo, and co-workers reported the synthesis of ligand-free $[Ag_2]^0$ clusters in the pores of a MOF with the formula of $Ni_2\{Ni_4[Cu_2(Me_3mpba)_2]_3\}\cdot 54H_2O$ [**1**] (Me_3mpba^{4-} = *N*,*N*′-2,4,6-trimethyl-1,3-phenylenebis(oxamate)),[18] and Ag_2@MOF was obtained by a two-step post synthetic process as specified below. In the first step, Ag-exchanged MOF [**2**] was obtained by immersing **1** in an aqueous solution of $AgNO_3$. In the second step, Ag_2 containing MOF [**3**] was obtained by reducing **2** with $NaBH_4$. The crystal structure of **3** was successfully solved, and ligand-free $[Ag_2]^0$ clusters were located in the pores of **3**. Compound **3** showed high catalytic activity in the Bunchner ring expansion reaction between toluene and ethyl diazoacetate, while **1** and **2** without the Ag cluster showed much lower activities. Still, the number of papers reporting the formation of small Ag clusters inside the pores of MOFs, especially mentioning their sizes, is limited. This limitation arises because MOFs are generally unstable under irradiation by an electron beam,[17] and it is difficult to observe the clusters by electron microscopes due to degradation of MOFs and sintering of clusters.

3. Silver clusters confined in zeolites

3.1. Silver-exchanged zeolites (Ag-zeolites)

Zeolites are porous crystalline aluminosilicates composed of covalently bonded tetrahedral TO_4 (T = Si, Al) units. The framework of zeolites, composed of TO_4 connections, can be of various structure types, and faujasite (FAU) and Linde type A (LTA) are well-known representative framework structures (Fig. 3).[19] Extra-framework cations (*e.g.*, Li^+, Na^+, K^+, NH_4^+, Ca^{2+}) reside within the pores of zeolites owing to the negatively charged nature of zeolite frameworks, depending on the Si/Al ratio. These extra-framework cations can be exchanged in solution with other metal cations. In particular, Ag-exchanged zeolites (Ag-zeolites) have been intensively studied since Ralek and co-workers first reported the unique color change of Ag-zeolites depending on the degree of hydration and Ag loading.[20] One of the first studies on the PL of Ag-zeolites was reported by Ozin and co-workers,[21] where blue and green emissions were observed in Ag-exchanged FAU with different Ag loadings. Later, Calzaferrin and co-workers reported the formation of luminescent quantum-sized Ag sulfide clusters in LTA.[22]

The unique luminescence properties of Ag-zeolites arise from small Ag clusters in zeolite scaffolds, which are activated with external stimuli. Cluster formation is initiated by reducing Ag^+ to Ag^0 in zeolite frameworks *via* loss of oxygen atoms from the zeolite framework (reaction (1))[4,23] and/or dehydration (reaction (2))[24,25]

$$2Ag^+ + ZO^{2-} \rightarrow 1/2O_2 + 2Ag^0 + Z \quad (1)$$

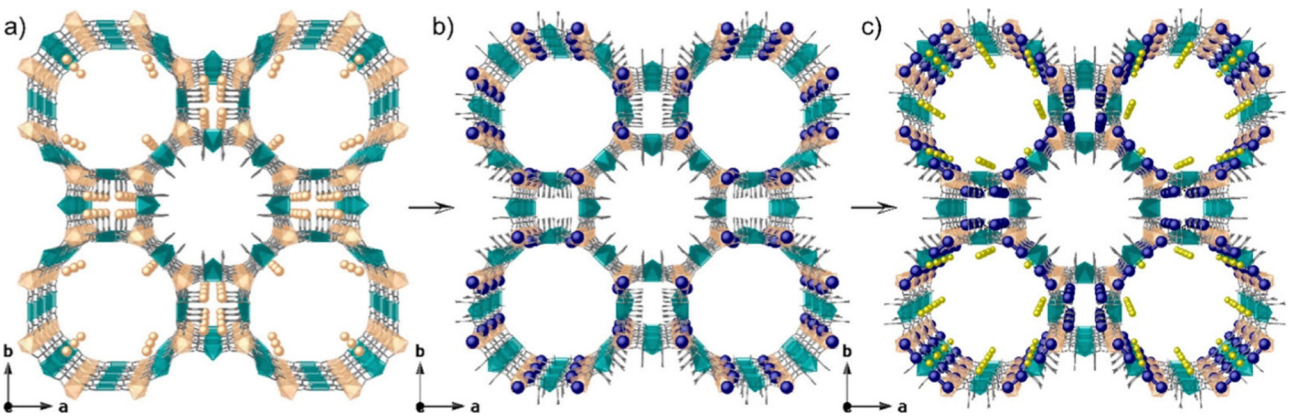

Fig. 2 Design approach showing the crystal structures of (a) **1**, (b) **2**, and (c) **3**, showing the two-step post-synthetic process of the formation of Ag_2@MOF. Cu and Ni atoms from the network are represented by cyan and orange polyhedra, respectively, whereas organic ligands are depicted as gray sticks. Orange, yellow, and blue spheres represent Ni, Na, and Ag atoms, respectively. Reprinted with permission from Tiburcio *et al.* Copyright 2022 American Chemical Society.

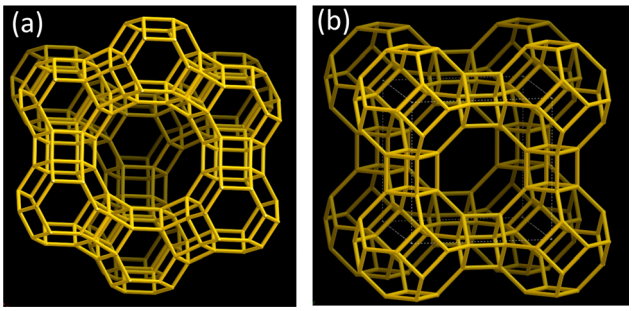

Fig. 3 Framework structure of (a) FAU and (b) LTA.[19] The Si–O–Si(Al) bonds are depicted as orange sticks.

$$Ag^{+} + H_2O \rightarrow 2H^{+} + 2Ag^{0} + 1/2O_2 \quad (2)$$

(where ZO^{2-} represents the zeolite framework highlighting one of its oxygen atoms, and Z represents the oxygen-deficient zeolite framework).

Monoatomic Ag^0, which form *via* reaction (1) and/or (2), subsequently self-assemblies with Ag^+, and small Ag clusters form in the zeolite cages. It has been widely recognized that zeolites are appropriate scaffolds for small Ag clusters because the Ag clusters can be stabilized in the zeolite frameworks *via* electrostatic interaction or coordination bond with the oxygen atoms, as well as the confinement effect. Meanwhile, to proceed reaction (1) and/or (2), external stimuli such as thermal treatment and light irradiation are needed, which will be introduced in the next section.

3.2. Synthetic approaches of small silver clusters in zeolites

Ag-zeolites can be activated by various methods to obtain Ag clusters, and thermal treatment is one of the most commonly used methods.[26–35] Upon thermal treatment, Ag-zeolites are heated gradually to prevent structure damage, and heating is kept for about a day after reaching the target temperature to produce Ag^0 by reaction (1) and/or (2). For example, Ag_4 clusters were formed in K-exchanged LTA (K-LTA) by heating partially Ag-exchanged K-LTA, which was pre-treated at 100 °C and 150 °C followed by heating to 450 °C and keeping overnight.[31] In addition, the atmosphere for thermal treatment may also affect the properties of Ag clusters. In particular, applying high vacuum shows activating effect *via* reaction (2), resulting in the formation of small Ag clusters with luminescent properties.[5,36]

Ag-zeolites can also be activated by irradiation with UV light,[37,38] electron beam,[39] X-ray,[40–42] or γ-ray.[43] Michalik and Kevan reported the formation of small Ag clusters in partially Ag-exchanged Na-LTA by γ-ray irradiation at 77 K, and the existence of linear $[Ag_3]^0$ and $[Ag_6]^+$ was suggested by electron spin resonance (ESR) measurement.[43] By activation with UV light, Ag clusters can be formed in irradiated spots with high space resolution. This method enables well-localized formation of luminescent small Ag clusters and could be applied to optical encoding.[38] Sasaki and Suzuki observed the formation and growth of Ag species in a zeolite scaffold from clusters of approximately 1 nm in size to much larger nanoparticles with electron beam irradiation of Ag-LTA and Ag-FAU.[39] The distribution of Ag clusters corresponded to the pore arrangement in the zeolite crystal, which means that the Ag clusters are formed in the pores of zeolites. Importantly, electron beam irradiation can initiate large cluster formation and overcome the energy barriers to particle growth, while thermal treatment may not. Fenwick and co-workers monitored the growth of Ag species in Ag-FAUX zeolite with X-ray irradiation and found that the growth dynamics obey the Hill–Langmuir equation.[42]

Chemical reduction is another activation method of Ag-zeolites.[44–46] For example, Shimizu and co-workers reported the formation of $[Ag_4]^{2+}$ in MFI zeolite, which formed independently of the degree of Ag-exchange, by the reduction of Ag-MFI with H_2 at 573 K.[45] The Ag clusters served as catalytically active sites for the reduction of NO by hydrocarbons (HC-SCR).[47]

3.3. The effect of parameters on the properties of silver cluster in zeolites

The main parameters to control the properties of small Ag clusters are as follows: (1) the topology of zeolite frameworks (LTA, FAU, MFI, *etc.*), (2) the charge of zeolite (Si/Al ratio), (3) Ag loading (degree of Ag-exchange), (4) the types or amounts of cations contained in the parent zeolite, (5) the degree of hydration, and (6) the activation method. Hereafter, we will introduce how these parameters affect the properties of small Ag clusters in zeolites by giving some representative examples.

3.3.1. The effect of topology/charge of zeolites and Ag loadings on the size of clusters. De Cremer, Sels, Vosch, and co-workers investigated the effects of the topology of zeolite framework and Ag loading on the PL properties by utilizing five parent zeolites (Na/K/Ca-LTA and FAUX/Y, where X and Y possess Si/Al ratio of <2 and >2, respectively) (Fig. 4).[27] To investigate the luminescent species formed in zeolite scaffolds, emission-excitation matrix (EEM) measurements were carried out for the five Ag-zeolites with different Ag loading after activation by calcination at 450 °C under air. Ag clusters of different sizes in each Ag-zeolite can be detected since a specific peak in the EEM corresponds to a particular luminescent species. Green-yellow and red emitting species were found in LTA zeolites when Ag loading was low and high, respectively (Fig. 4). On the other hand, Ag-FAUX/Y show green-yellow emissions regardless of Ag loading, suggesting that the size of Ag clusters formed in FAUX/Y is independent of Ag loadings.

Fenwick, Roeffaers, and co-workers investigated the effect of Ag loadings on the PLQY of Ag_x-FAUY (x = 0–6.5).[31] The PLQY increased with the decrease in Ag loadings and reached almost 100% at x = 0.5. To understand this phenomenon, extended X-ray absorption fine structure (EXAFS) spectroscopy was carried out, which revealed that the size of clusters and the proportion of Ag atoms involved in cluster formation remained almost constant (67% and 62% for $Ag_{0.5}$-FAUY and $Ag_{6.5}$-FAUY, respectively), indicating that these two factors are not the main parameters for the high PLQY of FAUY. On the other hand, the Debye–Waller factor associated with the Ag–Ag shells of $Ag_{0.5}$-FAUY (0.026) was much smaller than that of $Ag_{6.5}$-FAUY

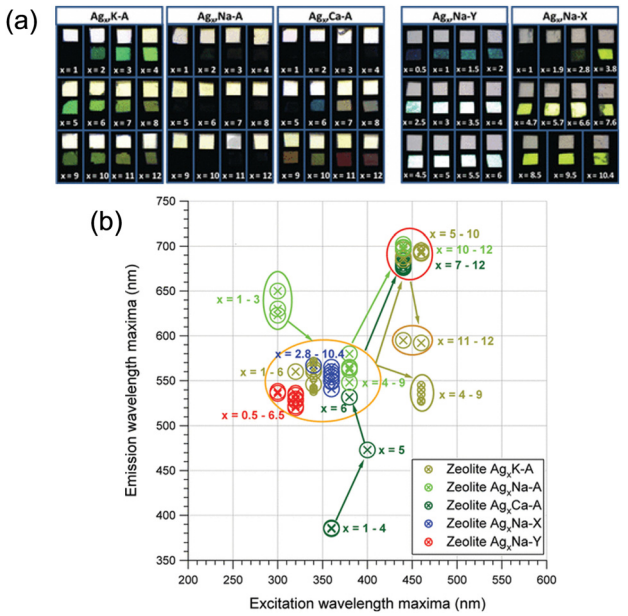

Fig. 4 (a) Photographs of Ag-exchanged zeolites after heat treatment. For each Ag loading, the upper picture represents the sample under room light illumination, while the lower picture is taken under UV illumination (360 nm). (b) Position of the most pronounced luminescence bands of the heat-treated Ag-exchanged zeolites. For each set of samples, the global trends upon increasing the Ag loading are highlighted by the colored arrows. Reprinted with permission from De Cremer *et al.* Copyright 2009 American Chemical Society.

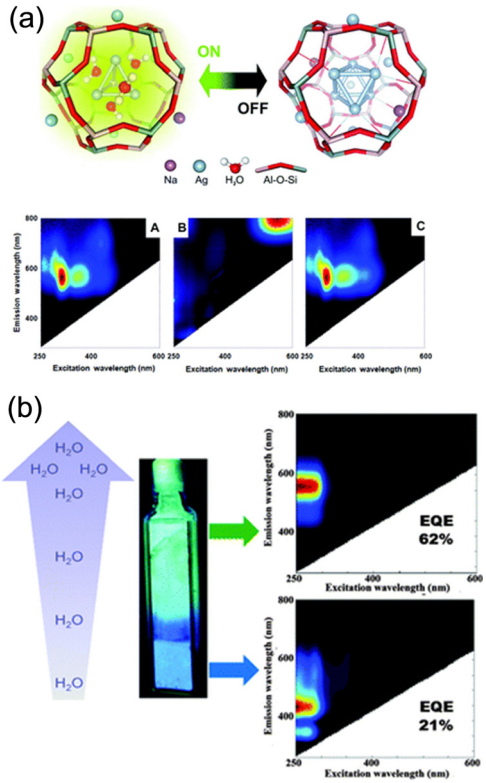

Fig. 5 (a) (top) Schematic representation of the reversible opto-structural switching of Ag clusters confined in partially Ag-exchanged Na-LTA. (bottom) 2D excitation–emission plots of the sample in the (left) hydrated, (middle) dehydrated, and (right) rehydrated state. Reprinted with permission from Aghakhani *et al.* Copyright 2018 Royal Society of Chemistry. (b) Water dependence of the emission color observed in Ag_1-LTA(Li). In fully hydrated samples, a green emission was found, whereas in partially hydrated samples blue emission was recorded. The water gradient observed in the cuvette was generated by leaving the materials exposed to air under ambient conditions. Reprinted with permission from Coutino-Gonzalez *et al.* Copyright 2015 Royal Society of Chemistry.

(0.044), indicating that Ag_4 in $Ag_{0.5}$-FAUY are significantly more ordered than the Ag_4 in $Ag_{6.5}$-FAUY. Therefore, the high PLQY of FAUY at low Ag loadings originates from the ordered structure of Ag clusters. It is noteworthy to comment that PLQY can be optimized to nearly 100% in FAUY, while FAUX, with the same topology but higher extra-framework cation (Na^+) content, showed very low PLQY. A detailed analysis of the EXAFS signal of Ag_1-FAUX revealed a sodium shell around the Ag clusters, which is not detected in FAUY. This fact suggests that Na^+, which is more concentrated and mobile in FAUX, plays a key role. Consequently, Na^+ can move inside the sodalite cages, interfering with Ag cluster formation and affecting their electronic/geometric structure.

To summarize, these results indicate that the luminescent properties of small Ag clusters are highly dependent on the topology of zeolite frameworks, the charge of zeolite (Si/Al ratio), and Ag loading.

3.3.2. The effect of hydration on the size of Ag clusters. The size of Ag clusters in zeolites is also influenced by the degree of hydration. For example, Aghakhani, Grandjean, and co-workers reported that green emitting $[Ag_4(H_2O)_4]^{2+}$ formed in partially Ag-exchanged Na-LTA transformed into dark (non-luminescent) water-free octahedral $[Ag_6]^{2+}$, which strongly interacts with the framework oxygen, upon dehydration at 450 °C under vacuum (Fig. 5a).[32] As the structural transformation is reversible, green emission is observed again after rehydration of the Ag-zeolite with $[Ag_6]^{2+}$, highlighting the high-contrast opto-structural switching of Ag cluster in zeolites.

Coutino-Gonzalez, Sels, and co-workers investigated the luminescence properties of Ag_x-LTA(Li) (x = 1–12), which is the Ag-exchanged form of Li_4Na_8-LTA after calcination at 450 °C.[30] As in the case of the composites reported by De Cremer and co-workers,[27] the samples showed green-yellow emissions at low Ag loadings ($x < 6$) and red emissions at high Ag loadings under hydrated conditions. In particular, at low Ag loadings (x = 1–4), an intense blue emission was observed in the partially hydrated state, while green/yellow emission was observed in the fully hydrated state (Fig. 5b). EXAFS analyses suggested that the blue and green/yellow emissions originate from Ag_3 and Ag_4, respectively.

Hoshino and co-workers investigated the PL properties of "air-packed samples" which is an Ag_{12}-LTA heated at 500 °C for 24 h under air for dehydration and packed in a glass cell with air at various temperatures, followed by cooling to room temperature to control the degree of hydration.[26] The samples packed at 100 °C exhibited an emission band, which was not observed for those packed at higher temperatures. *In situ* Ag *K*-edge EXAFS was measured to investigate the origin of the

emission band, which revealed the formation of $[Ag_5]^{m+}$ ($m \geqq 3$) for the samples air packed below 100 °C, since dark Ag_6 clusters were unstable in hydrated Ag_{12}-LTA.

All these results show that the cluster sizes (*e.g.*, Ag_3, Ag_4, Ag_5, and Ag_6) and the corresponding luminescence properties depend on the hydration level of zeolites.

3.3.3. The effect of types and amounts of extra-framework cations. This section introduces the effect of cations of the parent zeolite on the properties of Ag clusters. The mobility of metal ions as counter cations of the zeolite framework is affected by a trade-off between electrostatic cation-zeolite framework attractions and cation–cation repulsions. Fenwick and co-workers investigated the growth dynamics of Ag clusters in Ag-FAUX/Y zeolite under X-ray irradiation with Auger spectra.[42] In this study, the authors proposed to use the modified auger parameter (MAP), which is equal to the sum of the binding energy of Ag $3d_{5/2}$ electrons and the kinetic energy of Ag $M_4N_{4,5}N_{4,5}$ Auger electrons, to define whether the Ag species is metallic or not since the MAP values of metallic Ag, Ag^+, and Ag clusters differ. The MAP values of each sample plotted as a function of the X-ray dose show that the values change from ion/cluster to metallic ones at a critical X-ray dose. The critical X-ray doses of four composites (Ag_{11}-FAUX, $Ag_{6.5}$-FAUX, Ag_3-FAUY, and $Ag_{6.5}$-FAUY, where Ag_{11}-FAUX and $Ag_{6.5}$-FAUY are fully Ag-exchanged samples) show two trends: (1) Ag cluster in Ag-FAUX are more stable against X-ray exposure than those in FAUY, and (2) fully exchanged Ag-zeolites are more stable against X-ray exposure than partially exchanged ones. These trends can be related to the mobility of cations in the zeolite frameworks. That is, when the negative charge of the zeolite framework is increased (*i.e.*, from FAUY to FAUX), the electrostatic attraction between Ag^+ and the framework increases, decreasing the mobility of Ag^+. In addition, since cation–cation repulsion increases with the density of cations, the mobility of Ag^+ would decrease with the increase in Ag loading. Therefore, the Ag clusters in fully Ag-exchanged FAUX, with higher negative charge and Ag loading, should be more stable.

The size change of Ag clusters with hydration/dehydration, as mentioned above,[32] can also be considered as an example affected by the mobility of cations. Notably, the Ag clusters formed in calcined $NaAg_3$-LTA exist as Ag_4 (a mixture of 80% of $Ag_4(H_2O)_4$ and 20% of $Ag_4(O_{framework})_2$) and can be readily dehydrated to form dark $[Ag_6]^{2+}$. On the other hand, it is more difficult to dehydrate Ag_4 in calcined KAg_3-LTA (a mixture of 60% $[Ag_4(H_2O)_2]^{2+}$ and 40% of $[Ag_4(H_2O)_4]^{2+}$), resulting in the formation of emissive Ag_4 with high stability. The authors mentioned that this phenomenon may be due to the larger size and thus lower mobility of K^+ than Na^+, leading to preserve the coordination water molecules. We note that the origin of the PL of Ag_4 has been evaluated with time-dependent DFT calculations. Ag_4 exhibits a closed-shell electronic configuration, in which the Ag 4d shell is completely filled, and the two remaining 5s electrons are delocalized over the cluster. Upon excitation, one electron of the s-type HOMO is promoted to the p-type LUMO and relaxes through enhanced intersystem crossing into long-lived triplet states.[33]

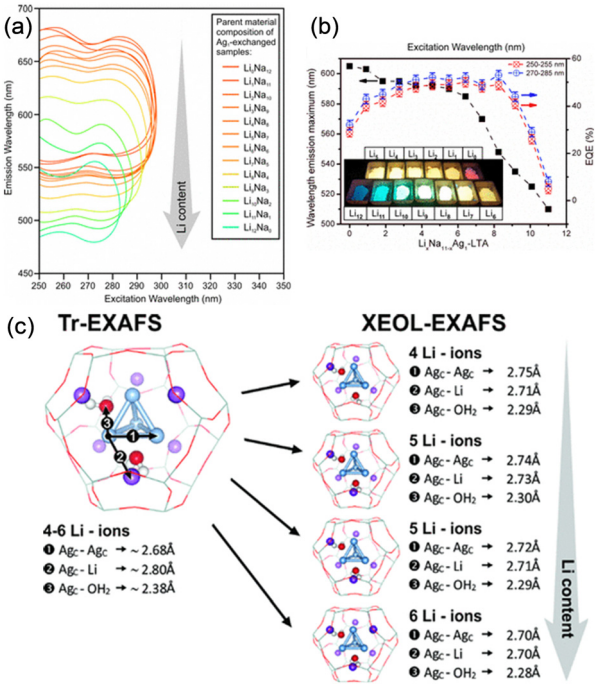

Fig. 6 (a) 2D emission and excitation profiles of the different hydrated Ag-exchanged LTA. (b) Maximal emission wavelength (excitation at 270–285 nm) and external quantum efficiency of the $Ag_1Li_xNa_{(11-x)}$-LTA depending on the Li content. (c) Schematic representation of the changes observed for the ground and excited states of the tetrahedral Ag clusters as determined by Tr- and XEOL-EXAFS, respectively. Reprinted with permission from Baekelant *et al.* Copyright 2018 American Chemical Society.

The counter cations of zeolites also affect the geometry of Ag clusters confined in the zeolite cages. As shown in Fig. 6, Baekelant, Steele, and co-workers investigated the luminescence properties of calcined $Ag_1Li_xNa_{(11-x)}$-LTA, prepared by introducing Ag^+ into Li-exchanged $Li_xNa_{(12-x)}$-LTA.[48] They reported that the emission color of calcined $Ag_1Li_xNa_{(11-x)}$-LTA continuously changes from red to blue with increased Li loading. X-ray-excited optical luminescence (XEOL) combined with EXAFS revealed that the bond length between the Ag of Ag_4 cluster and the O atoms of zeolite framework reduces with the increase in Li loading, causing the continuous emission color change.

4. Ag clusters confined in porous ionic crystals (Ag-PICs)

4.1. Porous ionic crystals

In this section, we will introduce synthetic approaches of small Ag clusters utilizing polyoxometalate-based porous crystalline solids. Polyoxometalates (POMs) are nanosized anionic metal-oxygen clusters, and Keggin ($[XM_{12}O_{40}]^{n-}$) and Dawson ($[X_2M_{18}O_{62}]^{n-}$) types are the widely used representative POMs. In recent years, POMs have been utilized as building blocks in combination with molecular macrocation to synthesize porous ionic crystals (PICs).[49,50] Generally, POMs have a high negative charge, and the framework structure of PICs composed of

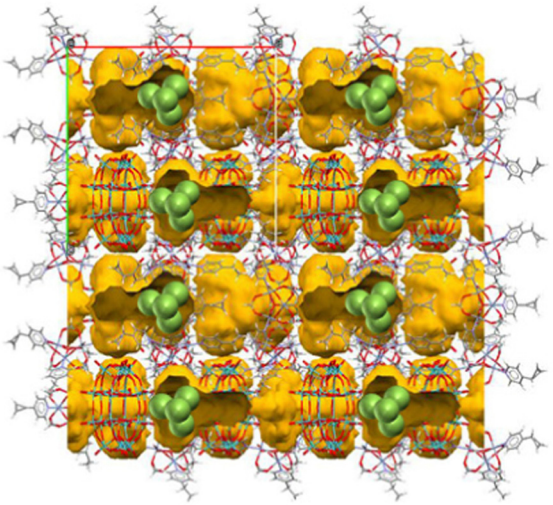

Fig. 7 A PIC scaffold with Dawson-type POM.[55] Yellow part indicates the closed pores of approximately 1.4 × 2.2 nm^2 in size. The pore size is sufficiently large to accommodate a Ag_4 cluster (green spheres indicate the Ag toms).

POMs and macrocations are negatively charged: the negative charge of the framework is compensated by exchangeable cations such as K^+, Cs^+, and NH_4^+, resulting in no net charge on the materials as a whole.[51] PICs possess ion-exchange properties, and Ag-exchanged PICs have been reported.[52] Additionally, PICs can serve as electron reservoirs since POMs show reversible redox-active properties based on the changes in the valence of composing metal ions.[53–55] Based on these observations, we have recently proposed to utilize PICs as scaffolds to form small Ag clusters based on their ion exchange and redox-active properties.[12–14] For instance, a PIC scaffold with Dawson-type POM contains closed pores of approximately 1.4 × 2.2 nm^2 in size,[55] sufficiently spacious to incorporate small Ag clusters, considering the van der Waals radius of Ag atoms (0.34 nm) (Fig. 7). As shown schematically in Fig. 8, upon soaking the reduced PICs into an aqueous solution of $AgNO_3$, the introduction and reduction of Ag proceed simultaneously, forming Ag clusters in the pores of PICs. Since the reduction of Ag^+ proceeds by the electron transfer from the reduced POM to Ag^+, this synthetic approach does not need any external stimuli or reducing reagents, which makes the operation simple. Therefore, this synthetic approach can be considered as a novel method to synthesize small Ag clusters.

4.2. Formation and stabilization of small Ag clusters in PICs

Cs^+ and electrons can be stored cooperatively in the PIC comprising $[PMo^{VI}_{12}O_{40}]^{3-}$ as follows, upon dispersing the PIC in water and adding CsCl and ascorbic acid as a reducing reagent (**red** stands for the reduced state)[53]

$$(mepyH)[Cr_3O(OOCH)_6(mepy)_3]_2[PMo^{VI}_{12}O_{40}]\ [\mathbf{I}] + e^- + Cs^+ \rightarrow Cs_2[Cr_3O(OOCH)_6(mepy)_3]_2[PMo^{VI}_{11}Mo^{V}O_{40}]\ [\mathbf{I\text{-}red\text{-}Cs}]\ (mepy = 4\text{-methylpyridine}) \quad (3)$$

Upon immersing **I-red-Cs**, which stores Cs^+ and electron *via* reaction (3), in an aqueous solution containing $AgNO_3$, ion-exchange between Cs^+ and Ag^+ and subsequent formation of Ag^0 by electron-transfer from the POM to Ag^+ occurs, followed by the self-assembly of the Ag species into small Ag clusters (reaction (4), **ox** stands for the oxidized state).[12]

$$Cs_2[Cr_3O(OOCH)_6(mepy)_3]_2[PMo^{VI}_{11}Mo^{V}O_{40}]\ [\mathbf{I\text{-}red\text{-}Cs}] + 2Ag^+ \rightarrow Ag^0Ag^I[Cr_3O(OOCH)_6(mepy)_3]_2[PMo^{VI}_{12}O_{40}] + 2Cs^+\ [\mathbf{I\text{-}ox\text{-}Ag}] \quad (4)$$

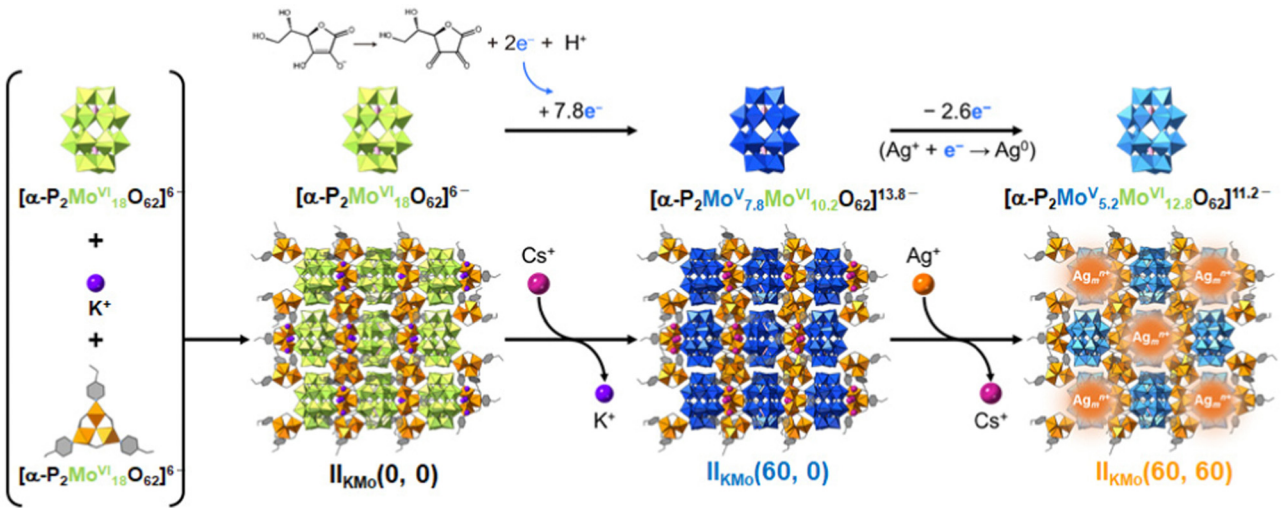

Fig. 8 Schematic representation of the Ag cluster formation in a PIC scaffold. Relationship among as-synthesized PIC ($\mathbf{II_{KMo}(0, 0)}$), reduction-induced ion-exchange of K^+ with Cs^+ ($\mathbf{II_{KMo}(60, 0)}$), and Ag incorporation followed by Ag cluster formation ($\mathbf{II_{KMo}(60, 60)}$). $\mathbf{II_{KMo}(t_1, t_2)}$ represents the PIC, which has been reduced and ion-exchanged with Cs^+ for t_1 min followed by the immersion in aqueous solution of $AgNO_3$ for t_2 min. Note that the number of transferred electrons with decimal points ($7.8e^-$ and $2.6e^-$) indicates bulk averages. Reprinted with permission from Haraguchi *et al.* Copyright 2023 Wiley-VCH.

On the other hand, simple ion-exchange (**IE**) between Cs^+ and Ag^+ occurs by immersing **I-ox-Cs**, which is obtained by oxidizing **I-red-Cs** with an aqueous solution of chlorine (reaction (5), ox stands for the oxidizing reagent), in an aqueous solution containing $AgNO_3$ (reaction (6)).

$$Cs_2[Cr_3O(OOCH)_6(mepy)_3]_2[PMo^{VI}{}_{11}Mo^{V}O_{40}]\ [\textbf{I-red-Cs}] + ox \rightarrow Cs[Cr_3O(OOCH)_6(mepy)_3]_2[PMo^{VI}{}_{12}O_{40}]\ [\textbf{I-ox-Cs}] + e^- + Cs^+ \quad (5)$$

$$Cs[Cr_3O(OOCH)_6(mepy)_3]_2[PMo^{VI}{}_{12}O_{40}]\ [\textbf{I-ox-Cs}] + Ag^+ \rightarrow Ag^{I}[Cr_3O(OOCH)_6(mepy)_3]_2[PMo^{VI}{}_{12}O_{40}] + Cs^+\ [\textbf{I-ox-AgIE}] \quad (6)$$

The reduction-induced ion-exchange (Fig. 9a, reaction (4)) occurs much faster than the simple ion-exchange (Fig. 9b, reaction (6)). **I-ox-Ag** is emissive while **I-ox-AgIE** is completely dark (Fig. 9c and d), suggesting the formation of small Ag clusters in **I-ox-Ag**. This difference clearly indicates that the formation of small Ag clusters was triggered by electron-transfer from the reduced POM to Ag^+ and the subsequent formation of Ag^0. Since a bright green emission is observed for $[Ag_4]^{2+}$ in zeolites,[33] formation of $[Ag_4]^{2+}$ is suggested in **I-ox-Ag**. This study demonstrates that PICs are promising candidates as scaffolds for the formation of small Ag clusters.

Because the activation sites for the commercial Ag/Al_2O_3 ethylene and propylene epoxidation catalyst are Ag_n (n = 2–4) clusters, we aimed to utilize the porosity and $[Ag_4]^{2+}$ in **I-ox-Ag** for the selective adsorption of unsaturated hydrocarbons. Gas adsorption studies have found that $[Ag_4]^{2+}$ exhibits high affinity toward acetylene and ethylene,[12] suggesting the potential of Ag cluster containing PICs as adsorbents and solid catalysts.

4.3. Analysis of the state of silver clusters by combining multiple measurements

In our previous study,[12] the assignment of Ag species ($[Ag_4]^{2+}$) was made based on the emission color (green) and composition. Therefore, further investigation is necessary to obtain detailed information on the states of Ag clusters in PICs. Hereafter, we will introduce a combination of techniques including PL, XPS, and XAFS measurements to investigate the state of Ag species in PICs. We utilized $K_3[Cr_3O(OOCH)_6(etpy)_3]_3[P_2W^{VI}{}_{18}O_{62}]$ [**II**] (etpy = 4-ethylpyridine) as a PIC scaffold to generate small Ag clusters *via* the following reactions.[13]

$$K_3[Cr_3O(OOCH)_6(etpy)_3]_3[P_2W^{VI}{}_{18}O_{62}]\ [\textbf{II}] + 5e^- + 5H^+ + 3Cs^+ \rightarrow Cs_3H_5[Cr_3O(OOCH)_6(etpy)_3]_3[P_2W^{VI}{}_{13}W^{V}{}_5O_{62}]\ [\textbf{II-red-Cs}] + 3K^+ \quad (7)$$

$$Cs_3H_5[Cr_3O(OOCH)_6(etpy)_3]_3[P_2W^{VI}{}_{13}W^{V}{}_5O_{62}]\ [\textbf{II-red-Cs}] + 3Ag^+ \rightarrow Ag_3H_{4.5}[Cr_3O(OOCH)_6(etpy)_3]_3[P_2W^{VI}{}_{15}W^{V}{}_3O_{62}]\ [\textbf{II-ox-Ag}] + 3Cs^+ + 0.5H^+ \quad (8)$$

Compound **II-ox-Ag** showed green emission similar to that of our previous work (**I-ox-Ag**),[12] suggesting the formation of Ag_4^{n+} (Fig. 10a and b). Then, we determined the oxidation state of Ag in **II-ox-Ag** by XPS. The narrow-scan XPS spectra of **II-ox-Ag** (Fig. 10c and d) suggest that 2 electrons were transferred from the reduced PIC to Ag^+ *via* reaction (8), and Ag^0 and Ag^+ existed in the ratio of 1 : 1. To gain information on the average size of the Ag cluster, XAFS measurement was carried out. The FT-EXAFS analysis revealed that the Ag atoms in **II-ox-Ag** have an average coordination number ($CN_{Ag–Ag}$) of 4.0, much smaller than $CN_{Ag–Ag}$ of the bulk sample ($CN_{Ag–Ag}$ = 12.6 obtained for Ag foil). This result indicates the formation of cluster-sized Ag species in **II-ox-Ag**. The Debye–Waller factor was small,

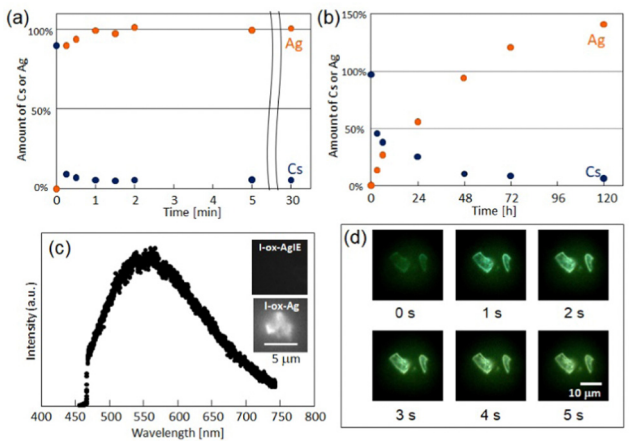

Fig. 9 Time course of the amounts of Cs or Ag in (a) reduction-induced ion-exchange and (b) simple ion-exchange reactions. (c) PL spectrum of **I-ox-Ag** with excitation at 405 nm and (d) time course of PL images. Reprinted with permission from Uchida *et al.* Copyright 2019 Royal Society of Chemistry.

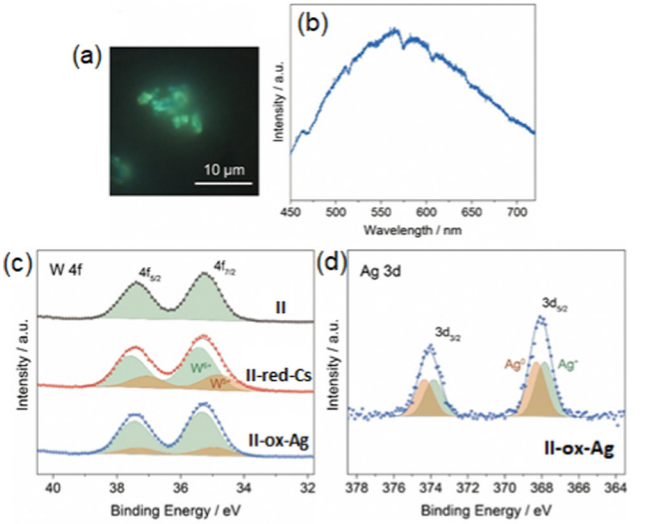

Fig. 10 PL (a) image and (b) spectrum of **II-ox-Ag** with excitation at 405 nm. Narrow scan XPS spectra (c) W 4f and (d) Ag 3d of with deconvolution. Reprinted with permission from Haraguchi *et al.* Copyright 2021 Wiley-VCH.

suggesting that the Ag cluster has a symmetric geometry. Based on these results, the Ag species in **II-ox-Ag** could be reasonably assigned to $[Ag_4]^{2+}$.[56,57] Besides, Ag–O was not clearly observed, indicating that the PIC contains ligand-free small Ag clusters, highlighting the uniqueness of this system.

4.4. Size-controlled synthesis of small Ag clusters in PICs with sole parameters

As summarized above, while Ag clusters of various sizes can be formed and stabilized in Ag-zeolite composites, which can be considered as analogues of Ag-PICs, the size of Ag clusters is only empirically controlled by parameters such as topology of zeolite structures, Ag loadings, type/amount of counter cations, temperature, heat treatment, and other activation methods. Therefore, our next objective was to strategically control the size of Ag clusters with parameters such as crystal structures, redox properties, reaction times, and counter cations of the PICs. Then, we employed isostructural redox-active PICs $A_3[Cr_3O(OOCH)_6(etpy)_3]_3[P_2M^{VI}{}_{18}O_{62}]$ (A = K or NH_4; M = Mo or W) as scaffolds to systematically investigate the parameters for controlling the Ag cluster size in PICs.[14] Hereafter, these PICs will be denoted as $II_{AM}(t_1, t_2)$. In this abbreviation, A and M show the counter cation (K^+ or NH_4^+) and metal elements contained in POMs (Mo or W), respectively, and t_1 and t_2 show the reaction times for reducing the PIC and Ag introduction, respectively.

Firstly, we synthesized small Ag clusters in a similar manner to our previous study (reaction (9) and (10)).[13] We note that the time for reduction (t_1) is a variable, which can control the degree of reduction (*i.e.*, the number of stored electrons in PICs), to investigate the effect of electron transfer from PICs to Ag^+ on cluster formation.

$$K_3[Cr_3O(OOCH)_6(etpy)_3]_3[P_2Mo^{VI}{}_{18}O_{62}] + xCs^+ + yH^+ + 7.8e^- \rightarrow Cs_{3.3}H_{7.5}[Cr_3O(OOCH)_6(etpy)_3]_3[P_2Mo^{V}{}_{7.8}Mo^{VI}{}_{10.2}O_{62}] \quad (t_1 = 60\ \text{min}) \quad (9)$$

$$Cs_{3.3}H_{7.5}[Cr_3O(OOCH)_6(etpy)_3]_3[P_2Mo^{V}{}_{7.8}Mo^{VI}{}_{10.2}O_{62}] + zAg^+ \rightarrow Ag_{3.9}H_{6.9}[Cr_3O(OOCH)_6(etpy)_3]_3[P_2Mo^{V}{}_{5.2}Mo^{VI}{}_{12.8}O_{62}] + 3.3Cs^+ \ (t_2 = 60\ \text{min}) \quad (10)$$

Then, we synthesized samples with long or short t_1 for the three isostructural PICs and characterized these samples to investigate the parameters influencing the cluster size. In Fig. 11, the PL spectra of samples with long t_1 (Fig. 11a–c, **II_{KMo}(60, 60)**, **II_{KW}(60, 60)**, and **II_{NH4Mo}(120, 60)**) and short t_1

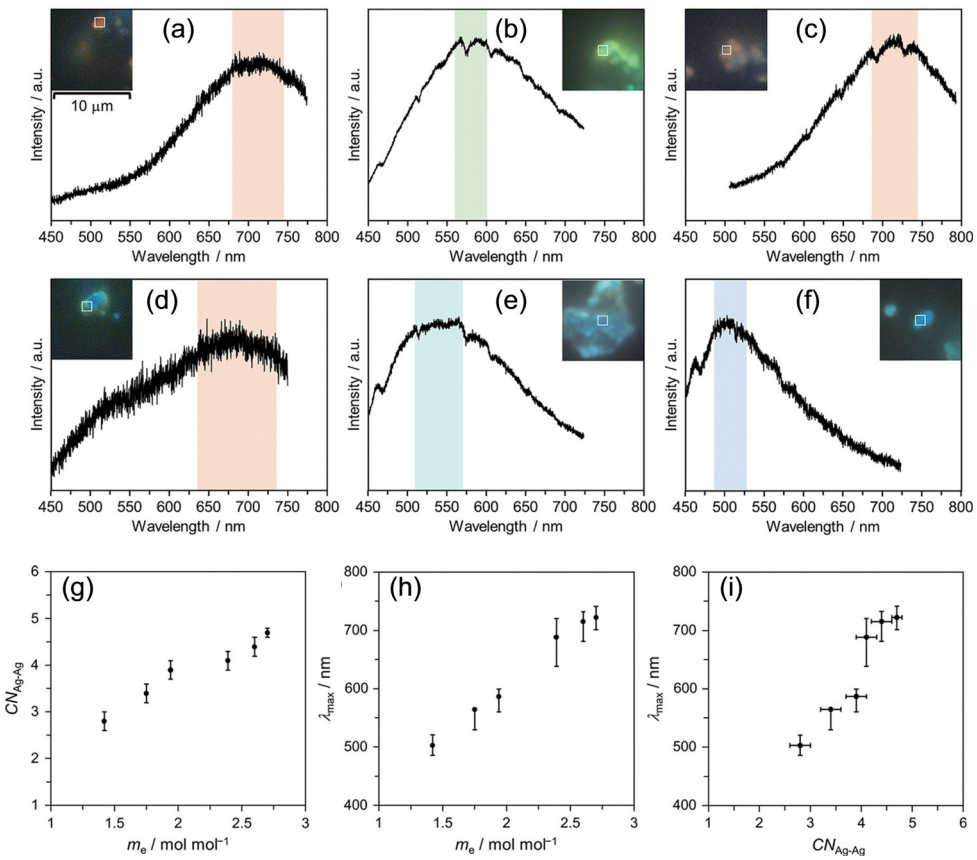

Fig. 11 PL images and spectra of (a) **II_{KMo}(60, 60)**, (b) **II_{KW}(60, 60)**, (c) **II_{NH4Mo}(120, 60)**, (d) **II_{KMo}(1, 60)**, (e) **II_{KW}(1, 60)**, and (f) **II_{NH4Mo}(5, 60)**. Each spectrum is the sum of PL emitted from the area indicated by the white open square. (g) CN_{Ag-Ag} *vs.* m_e (number of transferred electron), (h) λ_{max} *vs.* m_e, and (i) λ_{max} *vs.* CN_{Ag-Ag}. The error bar of λ_{max} is estimated by extracting the top 10% intensity range from the smoothed PL spectrum drawn by a moving average of five measurement points. Reprinted with permission from Haraguchi *et al.* Copyright 2023 Wiley-VCH.

(Fig. 11d–f, **II_{KMo}(1, 60)**, **II_{KW}(1, 60)**, and **II_{NH4Mo}(5, 60)**) are shown. By comparing samples with long and short t_1 for each PIC, we observed that the maximum emission wavelength (λ_{max}) is red-shifted with an increase in t_1. It is well known that λ_{max} of small Ag clusters generally red-shifts with increasing size.[58] Therefore, these results indicate that the cluster size formed in samples with longer t_1 is larger than those with shorter t_1 for all three PIC scaffolds (**II_{KMo}**, **II_{KW}**, and **II_{NH4Mo}**).

These findings indicate that the degree of electron transfer from PICs to Ag^+ influences the size of Ag clusters formed in PICs. To clarify this trend, we conducted XAFS and XPS to investigate the correlation between cluster size and degree of electron transfer. Fig. 11g–i show the trends of CN_{Ag-Ag} and λ_{max} as a function of the average amounts of electrons transferred from POM to Ag^+ in the PICs. These figures clearly illustrate that the size and emission color of the Ag clusters correlate with the degree of electron transfer. The combination of elemental analysis (Ag loading), XPS (Ag 3d, W 4f, and Mo 3d regions to obtain the degree of electron transfer from POM to Ag and charge balance in the chemical formula), and XAFS (CN of Ag clusters) measurements reveals that the blue, green, and red emissions observed in **II_{NH4Mo}(5, 60)**, **II_{KW}(60, 60)**, and **II_{KMo}(60, 60)/II_{NH4Mo}(120, 60)**, respectively, can be attributed to $[Ag_3]^+$, $[Ag_4]^{2+}$, and $[Ag_6]^{2+}$, respectively. Therefore, it is shown that Ag cluster size can be controlled with a sole parameter, the degree of electron transfer, in the Ag-PICs system.

5. Summary and outlook

In this perspective, we provided an overview and categorized small Ag clusters formed and stabilized in porous crystalline solids, namely MOFs, zeolites, and PICs. Future challenges in utilizing MOFs include the synthesis of ligand-free metal clusters, which could result in physical properties different from those of ligand-protected ones. In fact, ligand-free Au_{25} cluster was successfully synthesized in the pores of a MOF (UiO-66) through *in situ* self-assembly of Zr_6O_x clusters, $Au_{25}(Capt)_{18}$ (Capt = captopril), and benzene-1,4-dicarboxylate under ambient conditions followed by heating under vacuum.[59] The ligand-free Au_{25} cluster exhibited much superior stability and catalytic activity compared with the pristine clusters. This method could also be applied to stabilize ligand-free luminescent Ag clusters in MOFs. Regarding the zeolite scaffold, numerous studies mention the structure-function (luminescence) relationship, which will facilitate the development of rational design rules for luminescent base metal[60] and metal alloy clusters in zeolites.

The PIC scaffold, a relatively new member of the porous crystalline solids family, utilizes the redox property of POMs. The Ag cluster size is controlled by the degree of electron transfer from the POM to Ag^+. No external stimuli or reducing reagents are required, simplifying the Ag cluster synthesis method. In particular, the ligand-free Ag clusters formed in PIC scaffolds exhibit remarkable stability in the presence of air, maintaining their emission color even after one year.[14] However, the size distribution of these clusters is relatively larger than those formed in zeolite, and achieving greater homogeneity in size remains a challenge. Our future challenge is to synthesize monodisperse Ag clusters by investigating the kinetics of Ag cluster formation, considering factors such as the choice of synthetic solvents, reaction temperature, Ag content, and the method of reduction, whether by reagents, electrochemical, or photochemical methods.

Author contributions

All authors contributed to collecting information and writing the manuscript.

Conflicts of interest

There are no conflicts to declare.

Acknowledgements

This work was supported by the JSPS Grants-in-Aid for Scientific Research from MEXT of Japan (JP23K17952, JP22H04914, JP21K18975, and JP20H02750), the International Network on Polyoxometalate Science at Hiroshima University, JSPS Core-to-Core program, and the joint research program No. R03003 and R04020 of Molecular Photoscience Research Center, Kobe University. N. H. wishes to acknowledge support from JSPS research fellowship for Young Scientist (JP22J23130).

Notes and references

1 K. Yonesato, D. Yanai, S. Yamazoe, D. Yokogawa, T. Kikuchi, K. Yamaguchi and K. Suzuki, *Nat. Chem.*, 2023, **15**, 940–947.
2 Y. Chai, W. Shang, W. Li, G. Wu, W. Dai, N. Guan and L. Li, *Adv. Sci.*, 2019, **6**, 1900299.
3 J. Zheng, C. Zhang and R. M. Dickson, *Phys. Rev. Lett.*, 2004, **93**, 077402.
4 T. Sun and K. Seff, *Chem. Rev.*, 1994, **94**, 857–870.
5 R. Seifert, A. Kunzmann and G. Calzaferri, *Angew. Chem., Int. Ed.*, 1998, **37**, 1521–1524.
6 K. LaiHing, P. Y. Cheng and M. A. Duncan, *Z. Phys. D*, 1989, **13**, 161–169.
7 Z. Wu, E. Lanni, W. Chen, M. E. Bier, D. Ly and R. Jin, *J. Am. Chem. Soc.*, 2009, **131**, 16672–16674.
8 R. W. Huang, Y. S. Wei, X. Y. Dong, X. H. Wu, C. X. Du, S. Q. Zang and T. C. W. Mak, *Nat. Chem.*, 2017, **9**, 689–697.
9 X.-Y. Dong, H.-L. Huang, J.-Y. Wang, H.-Y. Li and S.-Q. Zang, *Chem. Mater.*, 2018, **30**, 2160–2167.
10 E. Coutiño-Gonzalez, W. Baskelant, J. A. Steele, C. W. Kim, M. B. J. Roeffaers and J. Hofkens, *Acc. Chem. Res.*, 2017, **50**, 2353–2361.
11 L. Sun, M. Keshavarz, G. Romolini, B. Dieu, J. Hofkens, F. de Jong, E. Fron, M. B. J. Roeffaers and M. Van der Auweraer, *Chem. Sci.*, 2022, **13**, 11560–11569.

12 S. Uchida, T. Okunaga, Y. Harada, S. Magira, Y. Noda, T. Mizuno and T. Tachikawa, *Nanoscale*, 2019, **11**, 5460–5466.
13 N. Haraguchi, T. Okunaga, Y. Shimoyama, N. Ogiwara, S. Kikkawa, S. Yamazoe, M. Inada, T. Tachikawa and S. Uchida, *Eur. J. Inorg. Chem.*, 2021, 1531–1535.
14 N. Haraguchi, N. Ogiwara, Y. Kumabe, S. Kikkawa, S. Yamazoe, T. Tachikawa and S. Uchida, *Small*, 2023, **19**, e2300743.
15 X. Y. Dong, Y. Si, J. S. Yang, C. Zhang, Z. Han, P. Luo, Z. Y. Wang, S. Q. Zang and T. C. W. Mak, *Nat. Commun.*, 2020, **11**, 3678.
16 R. W. Huang, X. Y. Dong, B. J. Yan, X. S. Du, D. H. Wei, S. Q. Zang and T. C. W. Mak, *Angew. Chem., Int. Ed.*, 2018, **57**, 8560–8566.
17 R. J. T. Houk, B. W. Jacobs, F. E. Gabaly, N. N. Chang, A. A. Talin, D. D. Graham, S. D. House, I. M. Robertson and M. D. Allendorf, *Nano Lett.*, 2009, **9**, 3413–3418.
18 E. Tiburcio, Y. Zheng, M. Mon, N. Martin, J. Ferrando Soria, D. Armentano, A. Leyva Perez and E. Pardo, *Inorg. Chem.*, 2022, **61**, 11796–11802.
19 Database of Zeolite Structures, **https://www.iza-structure.org/databases/**.
20 M. Rálek, P. Jírů, O. Grubner and H. Beyer, *Collect. Czech. Chem. Commun.*, 1962, **27**, 142–146.
21 G. A. Ozin, F. Hugues, S. M. Mattar and D. F. McIntosh, *J. Phys. Chem.*, 1983, **87**, 3445–3450.
22 D. Brühwiler, R. Seifert and G. Calzaferri, *J. Phys. Chem. B*, 1999, **103**, 6397–6399.
23 L. R. Gellens, J. V. Smith and J. J. Pluth, *J. Am. Chem. Soc.*, 1983, **105**, 51–55.
24 Y. Kim and K. Seff, *J. Am. Chem. Soc.*, 1978, **100**, 6989–6997.
25 Y. Kim and K. Seff, *J. Am. Chem. Soc.*, 1978, **100**, 3801–3805.
26 H. Hoshino, Y. Sannohe, Y. Suzuki, T. Azuhata, T. Miyanaga, K. Yaginuma, M. Itoh, T. Shigeno, Y. Osawa and Y. Kimura, *J. Phys. Soc. Jpn.*, 2008, **77**, 064712.
27 G. De Cremer, E. Coutiño-Gonzalez, M. B. J. Roeffaers, B. Moens, J. Ollevier, M. Van der Auweraer, R. Schoonheydt, P. A. Jacobs, F. C. De Schryver, J. Hofkens, D. E. De Vos, B. F. Sels and T. Vosch, *J. Am. Chem. Soc.*, 2009, **131**, 3049–3056.
28 G. De Cremer, E. Coutino-Gonzalez, M. B. Roeffaers, D. E. De Vos, J. Hofkens, T. Vosch and B. F. Sels, *ChemPhysChem*, 2010, **11**, 1627–1631.
29 A. Mayoral, T. Carey, P. A. Anderson, A. Lubk and I. Diaz, *Angew. Chem., Int. Ed.*, 2011, **50**, 11230–11233.
30 E. Coutino-Gonzalez, W. Baekelant, D. Grandjean, M. B. J. Roeffaers, E. Fron, M. S. Aghakhani, N. Bovet, M. Van der Auweraer, P. Lievens, T. Vosch, B. Sels and J. Hofkens, *J. Mater. Chem. C*, 2015, **3**, 11857–11867.
31 O. Fenwick, E. Coutino-Gonzalez, D. Grandjean, W. Baekelant, F. Richard, S. Bonacchi, D. De Vos, P. Lievens, M. Roeffaers, J. Hofkens and P. Samori, *Nat. Mater.*, 2016, **15**, 1017–1022.
32 S. Aghakhani, D. Grandjean, W. Baekelant, E. Coutino-Gonzalez, E. Fron, K. Kvashnina, M. B. J. Roeffaers, J. Hofkens, B. F. Sels and P. Lievens, *Nanoscale*, 2018, **10**, 11467–11476.
33 D. Grandjean, E. Coutiño-Gonzalez, N. T. Cuong, E. Fron, W. Baekelant, S. Aghakhani, P. Schlexer, F. D'Acapito, D. Banerjee, M. B. J. Roeffaers, M. T. Nguyen, J. Hofkens and P. Lievens, *Science*, 2018, **361**, 686–690.
34 E. Fron, S. Aghakhani, W. Baekelant, D. Grandjean, E. Coutino-Gonzalez, M. Van der Auweraer, M. B. J. Roeffaers, P. Lievens and J. Hofkens, *J. Phys. Chem. C*, 2019, **123**, 10630–10638.
35 E. Johan, Y. Kanda, N. Matsue, Y. Itagaki and H. Aono, *J. Lumin.*, 2019, **213**, 482–488.
36 T. Altantzis, E. Coutino-Gonzalez, W. Baekelant, G. T. Martinez, A. M. Abakumov, G. V. Tendeloo, M. B. Roeffaers, S. Bals and J. Hofkens, *ACS Nano*, 2016, **10**, 7604–7611.
37 G. De Cremer, Y. Antoku, M. B. J. Roeffaers, M. Sliwa, J. Van Noyen, S. Smout, J. Hofkens, D. E. De Vos, B. F. Sels and T. Vosch, *Angew. Chem., Int. Ed.*, 2008, **47**, 2813–2816.
38 G. De Cremer, B. F. Sels, J.-I. Hotta, M. B. J. Roeffaers, E. Bartholomeeusen, E. Coutiño-Gonzalez, V. Valtchev, D. E. De Vos, T. Vosch and J. Hofkens, *Adv. Mater.*, 2010, **22**, 957–960.
39 Y. Sasaki and T. Suzuki, *Mater. Trans.*, 2009, **50**, 1050–1053.
40 E. Coutino-Gonzalez, D. Grandjean, M. Roeffaers, K. Kvashnina, E. Fron, B. Dieu, G. De Cremer, P. Lievens, B. Sels and J. Hofkens, *Chem. Commun.*, 2014, **50**, 1350–1352.
41 K. Taiji, Y. Iso and T. Isobe, *J. Lumin.*, 2018, **196**, 214–220.
42 O. Fenwick, E. Coutino-Gonzalez, F. Richard, S. Bonacchi, W. Baekelant, D. de Vos, M. B. J. Roeffaers, J. Hofkens and P. Samori, *Small*, 2020, **16**, e2002063.
43 J. Michalik and L. Kevan, *J. Am. Chem. Soc.*, 1986, **108**, 4247–4253.
44 L. R. Gellens, W. J. Mortier and J. B. Uytterhoeven, *Zeolites*, 1981, **1**, 85–90.
45 K.-i Shimizu, K. Sugino, K. Kato, S. Yokota, K. Okumura and A. Satsuma, *J. Phys. Chem. C*, 2007, **111**, 1683–1688.
46 A. Baldansuren, H. Dilger, R.-A. Eichel, J. A. van Bokhoven and E. Roduner, *J. Phys. Chem. C*, 2009, **113**, 19623–19632.
47 A. Satsuma, J. Shibata, K.-I. Shimizu and T. Hattori, *Catal. Surv. Asia*, 2005, **9**, 75–85.
48 W. Baekelant, S. Aghakhani, E. Coutino-Gonzalez, K. Kennes, F. D'Acapito, D. Grandjean, M. Van der Auweraer, P. Lievens, M. B. J. Roeffaers, J. Hofkens and J. A. Steele, *J. Phys. Chem. Lett.*, 2018, **9**, 5344–5350.
49 S. Uchida, *Chem. Sci.*, 2019, **10**, 7670–7679.
50 Y. Shimoyama and S. Uchida, *Chem. Lett.*, 2021, **50**, 21–30.
51 A. Lesbani, R. Kawamoto, S. Uchida and N. Mizuno, *Inorg. Chem.*, 2008, **47**, 3349–3357.
52 S. Uchida, R. Kawamoto, H. Tagami, Y. Nakagawa and N. Mizuno, *J. Am. Chem. Soc.*, 2008, **130**, 12370–12376.
53 R. Kawahara, S. Uchida and N. Mizuno, *Chem. Mater.*, 2015, **27**, 2092–2099.
54 S. Seino, R. Kawahara, Y. Ogasawara, N. Mizuno and S. Uchida, *Angew. Chem., Int. Ed.*, 2016, **55**, 3987–3991.
55 S. Hitose and S. Uchida, *Inorg. Chem.*, 2018, **57**, 4833–4836.
56 Ideally, a tetrahedral Ag_4 cluster should have a CN of 3 and not 4. The assignment (Ag_4) was made based on the

following information: (i) many papers indicate that green emission is observed for Ag4 clusters, while larger clusters (*e.g.*, Ag_6) shows reddish emission, (ii) the bulk sample gave a CN of 12.6, which is larger than the ideal value of 12, and (iii) PXRD and XPS measurements suggest that a small amount of bulk Ag has formed on the surface of the particles which may contribute to increase the CN.

57 It has been recognized that Ag-zeolite is sensitive to electron beam and X-ray irradiation. The CN obtained from EXAFS tends to be larger than the actual value because Ag clusters further sinters by electron beam and X-ray irradiation. Recently, efforts have been made to directly obtain structural information of luminescent species by using X-ray excited optical luminescence (XEOL)-XAFS[33].

58 A. Gonzalez-Rosell, C. Cerretani, P. Mastracco, T. Vosch and S. M. Copp, *Nanoscale Adv.*, 2021, **3**, 1230–1260.

59 H. Wang, X. Liu, W. Yang, G. Mao, Z. Meng, Z. Wu and H. L. Jiang, *J. Am. Chem. Soc.*, 2022, **144**, 22008–22017.

60 W. Baekelant, S. Aghakhani, E. Coutino-Gonzalez, D. Grandjean, K. Kennes, D. Jonckheere, E. Fron, F. d'Acapito, A. Longo, P. Lievens, M. B. J. Roeffaers and J. Hofkens, *J. Phys. Chem. C*, 2018, **122**, 13953–13961.